Flat-band ferromagnetism in quantum dot superlattices

Hiroyuki Tamura,[1] Kenji Shiraishi,[2] Takashi Kimura,[1] and Hideaki Takayanagi[1]
[1]*NTT Basic Research Laboratories, NTT Corporation, Atsugi, Kanagawa, 243-0198 Japan*
[2]*Institute of Physics, University of Tsukuba, Tsukuba, Ibaraki 305-2635, Japan*
(Received 27 April 2001; revised manuscript received 7 September 2001; published 8 February 2002)

The possibility of flat-band ferromagnetism in quantum dot arrays is theoretically discussed. By using a quantum dot as a building block, quantum dot superlattices are possible. We consider dot arrays on Lieb and *kagomé* lattices known to exhibit flat-band ferromagnetism. By performing an exact diagonalization of the Hubbard Hamiltonian, we calculate the energy difference between the ferromagnetic ground state and the paramagnetic excited state, and discuss the stability of the ferromagnetism against the second-nearest-neighbor transfer. We calculate the dot-size dependence of the energy difference in a dot model and estimate the transition temperature of the ferromagnetic–paramagnetic transition, which is found to be accessible within the present fabrication technology. We point out advantages of semiconductor ferromagnets and suggest other interesting possibilities of electronic properties in quantum dot superlattices.

DOI: 10.1103/PhysRevB.65.085324 PACS number(s): 73.63.Kv, 75.75.+a, 71.10.Fd

I. INTRODUCTION

Recent progress in the fabrication technology in nanoscale (''nanotechnology'') has enabled us to make various types of small devices using semiconductor quantum dots. Single electron transistors are one of the important examples of device application.[1] When the charging energy of a small quantum dot (artificial atom) is larger than the thermal energy, electrons in the lead cannot transfer into the dot due to the Coulomb blockade effect. By combining several single electron transistors, logic circuits are proposed.[2] By coupling several quantum dots, it is suggested that a qubit for quantum computation can be realized by controlling excess spins in coupled quantum dots.[3] Single electron transistors through coupled dots (artificial molecule) are also proposed, where a transition between the bonding and antibonding states serves as a qubit of quantum computation.[4,5]

Arrays of quantum dots have also been studied extensively; the quantum dot laser is one of the promising devices.[6] Recently, a self-organizing technique of quantum dots[7] enabled us to synthesize very small dots in well-ordered lattices.[8] In quantum dot lasers, electrons do not transfer between dots in general and interdot coupling seems unimportant. The quantum cellular automaton[9] is a very fascinating proposal for a dot array device utilizing electron transfer inside a cell of coupled dots and electrostatic force between the neighboring cells. Logical circuits using quantum cellular automata have been also proposed.[10] Magnetic properties of coupled dots have also been studied. A possibility of observing spontaneous magnetization has been proposed in arrays of strained quantum dots and potential applications in information storage and processing have been discussed.[11] It has also been shown that a square lattice of four coupled quantum dots containing 40 electrons has a ferromagnetic ground state.[12]

Recently, the present authors have proposed a type of device forming a superlattice of quantum dots.[13] If we consider a quantum dot as a building block and put it on a site of the lattice, we can create an artificial crystal having interesting properties.[14] In the dot lattice, we can design any type of lattice structure that we like regardless of the number of electrons in it. Lieb[15] and *kagomé*[16] lattices are interesting examples of such artificial lattices, because they have a dispersionless subband (flat band) in their single-particle band structures.[17] It has been proven that, in the repulsive Hubbard model of these lattices, ferromagnetism appears. Interestingly, it has been shown that the ferromagnetic spin wave has a finite stiffness below a Stoner gap[18] and that the ferromagnetism is robust against a finite dispersion.[19] Some other types of flat-band ferromagnetism have been proposed by several authors.[20–22] After their predictions, there have been several proposals to realize flat-band ferromagnetism based on real materials, such as carbon networks,[23,24] a graphite ribbon,[25,26] and Ga[27] and As[28] atomic wires. However, there has been no clear evidence of the observation of flat-band ferromagnetism, because it is difficult to form these lattices using the above materials since a lattice distortion effect would destabilize the ferromagnetism when the flat band is half-filled.[29] In real materials, the number of valence electrons is determined in such a way that the crystal structure is stable. Then, unrestricted material design is difficult in general.

On the other hand, dot lattices do not have such disadvantages. One can design various types of lattice structures. The spatial position is fixed because an artificial atom is in a rigid buried region in semiconductors. The dot lattice does not undergo structural deformations by electronic effects such as the Jahn-Teller distortion. Then, one can design lattice structures which do not exist in nature without worrying about the lattice instability. Moreover, the number of electrons in it can be changed in a controllable manner. By putting a gate electrode in the spatially separated region on top of the electron gas, it is easy to modify the electron filling over a wide range by changing the gate voltage.[30]

In Ref. 13, it was suggested that flat-band ferromagnetism might be observable in quantum dot arrays based on a simple calculation of a single-particle Hamiltonian. However, its feasibility in real experiments has been unclear, because the critical temperature in actual dot arrays was unknown. Moreover, the next-nearest-neighbor transfer that inevitably oc-

curs in real dot arrays could significantly reduce the critical temperature because it would destroy the flat band. For further consideration, a more sophisticated calculation is required that takes into account the Coulomb interaction and the next-nearest-neighbor transfer in a realistic dot model. In the present paper, we demonstrate that the flat-band ferromagnetism, which has been thought to be an artifact in a mathematical model, is actually observable at reasonable temperatures in dot arrays using existing fabrication technology.

In this paper, we discuss the possibility of realizing flat-band ferromagnetism in quantum dot superlattices. In Sec. II, we consider two types of two-dimensional (2D) dot lattices (Lieb and *kagomé* lattices) and obtain single-particle band structures using a tight-binding approximation including the next-nearest-neighbor transfer. In Sec. III, we diagonalize a Hubbard Hamiltonian for these lattices and obtain the energy difference of the ferromagnetic ground state and the paramagnetic excited state. In Sec. IV, we describe our quantum dot model. By calculating the transfer and on-site Coulomb energy, we obtain the size dependence of the energy difference and discuss the stability of the ferromagnetic ground state. In Sec. V, we argue that the magnetization can be expected in 2D dot lattices in spite of the famous Mermin-Wagner theorem. We indicate some device applications for semiconductor ferromagnets and propose other possibilities of dot superlattices having interesting electrical properties like superconductivity. Conclusions are presented in Sec. VI.

II. TIGHT-BINDING APPROXIMATION

We consider two types of lattices. Figure 1(a) shows the Lieb lattice and Fig. 1(b) the *kagomé* lattice. The Lieb lattice is a bipartite lattice which consists of two sublattices. Sites belonging to one sublattice are connected to sites belonging to another sublattice.[15] The *kagomé* lattice is a line graph of the hexagonal lattice.[16] We consider a Hubbard model,

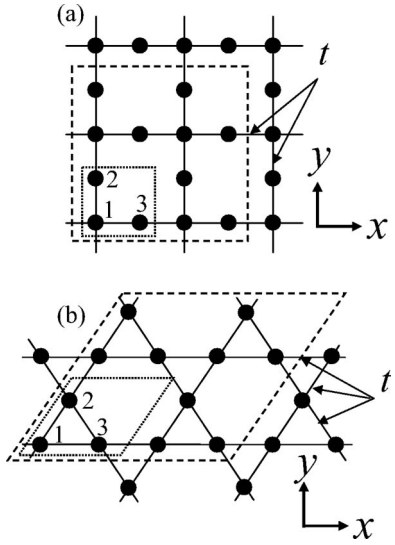

FIG. 1. The Lieb lattice (a) and *kagomé* lattice (b). Solid lines represent the nearest-neighbor transfer t. Dotted and dashed lines indicate one and 2×2 unit cell(s), respectively. A unit cell contains three sites $i=1$, 2, and 3.

$$H=-t\sum_{(i,j)\sigma}c_{i\sigma}^{+}c_{j\sigma}-t'\sum_{\langle i,k\rangle\sigma}c_{i\sigma}^{+}c_{k\sigma}+U\sum_{i}n_{i\uparrow}n_{i\downarrow}, \quad (1)$$

where t is the transfer between a pair (i,j) of the nearest-neighboring sites i and j, t' is the transfer between a pair $\langle i,k\rangle$ of the next-nearest-neighboring sites i and k, U is the on-site Coulomb energy on the site i, $c_{i\sigma}^{+}$ $(c_{i\sigma})$ is the creation (annihilation) operator of an electron on the site i with spin $\sigma=\uparrow$ or $\downarrow$, and $n_{\sigma}=c_{i\sigma}^{+}c_{i\sigma}$. In the noninteracting case $U=0$, we obtain the following tight-binding Hamiltonian equations of single-particle energy E for the Lieb lattice,

$$E\mathbf{c}=-t\begin{bmatrix}0 & 1+e^{-2ik_1a} & 1+e^{-2ik_2a}\\ 1+e^{2ik_1a} & 0 & 0\\ 1+e^{2ik_2a} & 0 & 0\end{bmatrix}\mathbf{c}-t'\begin{bmatrix}0 & 0 & 0\\ 0 & 0 & (1+e^{-2ik_1a})(1+e^{2ik_2a})\\ 0 & (1+e^{2ik_1a})(1+e^{-2ik_2a}) & 0\end{bmatrix}\mathbf{c}, \quad (2)$$

and for the *kagomé* lattice,

$$E\mathbf{c}=-t\begin{bmatrix}0 & 1+e^{-2ik_1a} & 1+e^{-2ik_2a}\\ 1+e^{2ik_1a} & 0 & 1+e^{2i(k_1-k_2)a}\\ 1+e^{2ik_2a} & 1+e^{-2i(k_1-k_2)a} & 0\end{bmatrix}\mathbf{c}$$
$$-t'\begin{bmatrix}0 & e^{-2i(k_1-k_2)a}+e^{-2ik_2a} & e^{-2ik_1a}+e^{2i(k_1-k_2)a}\\ e^{2i(k_1-k_2)a}+e^{2ik_2a} & 0 & e^{2ik_1a}+e^{-2ik_2a}\\ e^{2ik_1a}+e^{-2i(k_1-k_2)a} & e^{-2ik_1a}+e^{2ik_2a} & 0\end{bmatrix}\mathbf{c}, \quad (3)$$

where a is the interdot spacing, $\mathbf{k}=k_1\mathbf{b}_1+k_2\mathbf{b}_2$ is the wave vector expressed by the reciprocal-lattice vectors $\mathbf{b}_1$ and $\mathbf{b}_2$ (see insets of Fig. 2), and $\mathbf{c}=(c_1,c_2,c_3)$ are the amplitudes of the wave function at the site $i=1,2,3$ in the unit cell shown in Fig. 1. For $t'=0$, eigenvalues for Eqs. (2) and (3) are simply given by

$$E=0,\ \pm2t\sqrt{\cos^2(k_1a)+\cos^2(k_2a)} \quad (4)$$

for the Lieb model, and by

$$E=2t,\ \ t(-1\pm\sqrt{3+2\cos(2k_1a)+2\cos(2k_2a)+2\cos(2k_1a-2k_2a)}) \tag{5}$$

for the *kagomé* model. Figures 2(a) and 2(b) are the band diagrams for Lieb and *kagomé* lattices. For $t'=0$, dispersionless flat subbands are formed in the middle for the Lieb lattice and in the top for the *kagomé* lattice. When the next nearest transfer is taken into account ($t'>0$), the flat subbands are broken down, except for $2k_1a=\pi$ (from the X point to the M point) in the Lieb lattice. This is because the next-nearest transfers between site 2 and 3 are canceled between different unit cells.

III. EXACT DIAGONALIZATION

We diagonalize the Hubbard Hamiltonian (1) for 2×2 unit cells of 12 dots enclosed by dashed lines in Fig. 1. For the Lieb lattice, we use an antiperiodic boundary condition in the x direction and a periodic boundary condition in the y direction in order to avoid unimportant finite-size effects of additional degeneracy at the cross point of the flat band and dispersive bands. For the *kagomé* lattice, we use an ordinary periodic boundary condition.

Figure 3 shows the total spin as a function of the number of electrons N and U/t in the [Fig. 3(a)] Lieb and the [Fig. 3(b)] *kagomé* lattices for $t'=0$. For any $U/t>0$, high-spin states appear at the half-filling ($N=12$) for the Lieb lattice and $19\leqslant N\leqslant 22$ for the *kagomé* lattice. This result is consistent with the theorems proved by Lieb[15] for the Lieb lattice and Mielke[16] for the *kagomé* lattice. This result shows that the ferromagnetic state appears in a wide range of electrons filling in the *kagomé* lattice, whereas ferromagnetism appears only at the half-filling for the Lieb lattice. High-spin states seen in Fig. 3 when the Fermi level is not at the flat band ($N\neq12$ for the Lieb lattice and $N<16$ for the *kagomé* lattice) are due to an unimportant finite-size effect due to additional degeneracy.

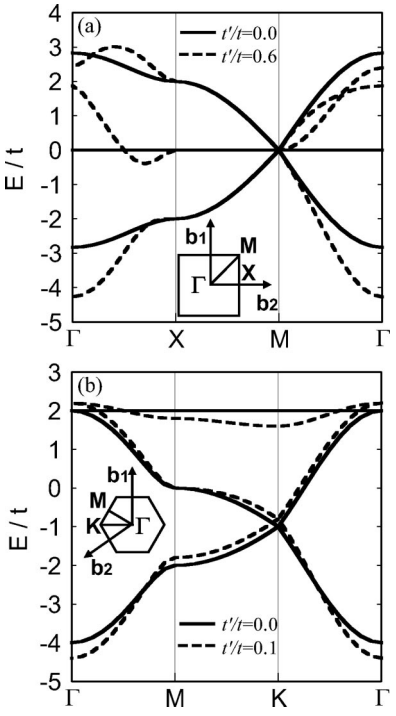

FIG. 2. Single-particle band energy E for (a) the Lieb lattice and (b) the *kagomé* lattice for the next-nearest-neighbor transfer $t'=0$ (solid line) and $t'>0$ (dashed line) calculated using the tight-binding approximation, where E and t' are normalized in units of the nearest-neighbor transfer t. Insets: Brillouin zone. $\mathbf{b}_1$ and $\mathbf{b}_2$ are the reciprocal-lattice vectors.

Figure 4 shows the energy difference between the ground state with spin $S=2$ and the lowest excited state with spin $S=0$ for various t's when the flat band is half-filled, i.e., [Fig. 4(a)] $N=12$ for the Lieb and [Fig. 4(b)] $N=20$ for the *kagomé* lattice. This energy difference can be regarded as a qualitative estimate of the transition temperature of ferromagnetic and paramagnetic transitions in a macroscopic sample as will be discussed in Sec. V. First we consider $t'=0$. As Lieb has already pointed out,[15] the high-spin state in

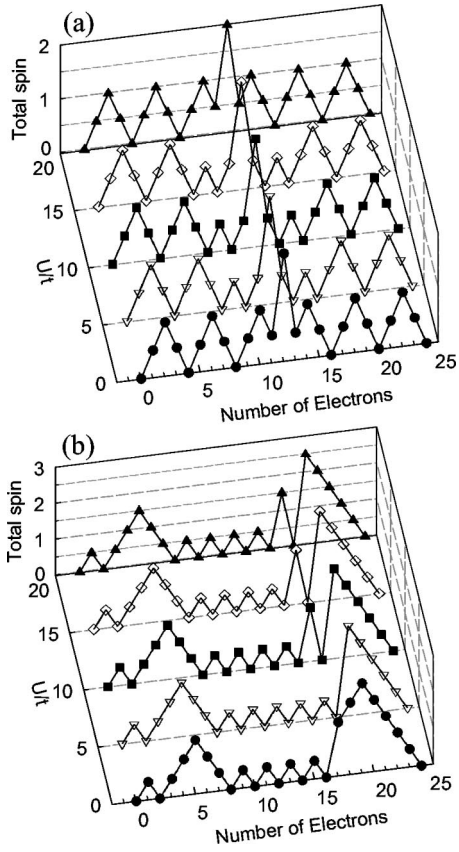

FIG. 3. Total spin as a function of the number of electrons $0\leqslant N\leqslant 24$ for $U/t=10^{-3}$, 5, 10, 15, and 20 for (a) the Lieb lattice and (b) the *kagomé* lattice when $t'=0$.

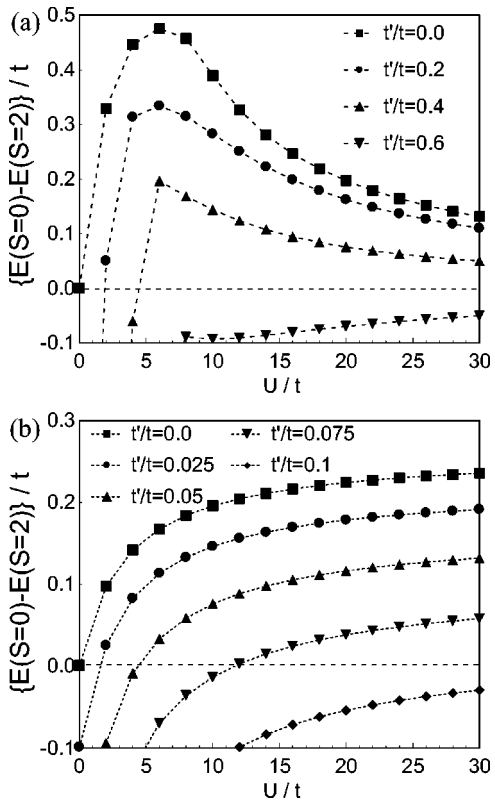

FIG. 4. Energy difference $E(S=0)$ and $E(S=2)$ as a function of U/t in (a) the Lieb ($N=12$) and (b) the *kagomé* lattices ($N=20$) for various values of t'.

the Lieb lattice is caused by the antiferromagnetic ordering at the half-filling. This ordering can be easily understood when $U/t \gg 1$. In this limit at the half-filling, there is one localized electron per dot. Due to the second-order process of an electron with up spin transferring to the neighboring dot having a down-spin electron, the effective exchange energy is given by $-2t^2/U$. As the numbers of sites in two sublattices are different, the remaining total spin is responsible for the ferromagnetism. The high spin in the *kagomé* lattice is caused by an effective exchange interaction of the third-order process cycling and exchanging two electrons with the opposite spins within the triangular lattice of three sites.[20] When $U/t \gg 1$, the energy loss due to this ring exchange is of the order of t, whereas there is no energy loss between two electrons with the same spins. Actually, from Fig. 4, one can deduce $\Delta E \simeq 4.3t^2/U$ for the Lieb lattice and $\Delta E \simeq 0.26t$ for the *kagomé* lattice, which is consistent with the above argument. When U/t is small, the energy difference is proportional to U in both cases, i.e., $\Delta E \simeq 0.16U$ for the Lieb lattice and $\Delta E \simeq 0.05U$ for the *kagomé* lattice. This is because the Coulomb repulsion raises the energy of the order of U when electrons on the flat band have the opposite spins in the lowest-spin state, whereas, by the Pauli principle, it does not when electrons on the flat band have the same spins in the high-spin state.

As t' is increased, the energy difference becomes smaller or sometimes negative. For small U/t, the ferromagnetic ground state for $t'=0$ is easily broken down by very small t', because the subband is no longer flat for $t'>0$ as seen in Fig. 2. Electrons are filled in such way as to lower the total spin to gain the single-particle energy of the order of t' rather than to align spins to gain the smaller exchange energy of the order of U. As U/t is increased, the gain from the effective exchange energy ΔE overcomes the loss from the single-particle energy which is of the order of t', and the ferromagnetic ground state becomes robust against t'. In the Lieb lattice, the ground state is always paramagnetic when $t'>0.6$ in the range $0<U/t<30$, whereas, in the *kagomé* lattice, the ferromagnetism disappears for $t'>0.1$. This difference in the robustness against t' comes from the magnitude of the effective exchange energy ΔE as seen in Fig. 4. When $U/t<1$, $\Delta E \simeq 0.16U$ for the Lieb lattice is much larger than $\Delta E \simeq 0.05U$ for the *kagomé* lattice. For $U/t \gg 1$, the antiferromagnetic exchange energy between the next-nearest-neighbor sites in the Lieb lattice slowly increases as $(t'/t)^2$ because $t'^2/U=(t'/t)^2(t^2/U)$, whereas, in the *kagomé* lattice, the ferromagnetic energy due to the ring exchange rapidly decreases as t'/t.

IV. QUANTUM DOT MODEL

To evaluate the transfer and on-site Coulomb energy for quantum dot arrays, we assume that electrons are confined in a two-dimensional confinement potential given by

$$V(\mathbf{r})=\sum_i v(\mathbf{r}-\mathbf{R}_i),$$

$$v(\mathbf{r})=\begin{cases} -\dfrac{1}{16}m^*\omega^2a^2[\cos(\pi x/a)\cos(\pi y/a)]^2 \\ \qquad \text{for } r<a/2, \\ 0 \qquad \text{for } r\geqslant a/2, \end{cases} \tag{6}$$

where m^* is the effective mass of an electron, ω is the confining oscillator frequency, $\mathbf{R}_i$ is the position of the ith dot, and a is the interdot spacing. This dot model is quite similar to that used for the square lattice.[31] Noting that $[\cos(\pi x/a)\cos(\pi y/a)]^2 \simeq [(2r/a)^2-1]^2 \simeq 1-2(2r/a)^2$ for $r \ll a/2$, the "atomic" wave function localized in the potential $v(\mathbf{r})$ is given in a good aproximation by

$$\phi(\mathbf{r})=\frac{2}{\sqrt{\pi}d}\exp\left(-\frac{2r^2}{d^2}\right), \tag{7}$$

where $d=2\sqrt{\hbar/m^*\omega}$ is the dot diameter.

The transfer and on-site Coulomb energies are given by

$$t(\mathbf{R}_i,\mathbf{R}_j)=-\int d\mathbf{r}\phi(\mathbf{r}-\mathbf{R}_i)\{-\hbar^2\nabla^2/2m^*+V(\mathbf{r})\} \times\phi(\mathbf{r}-\mathbf{R}_j), \tag{8}$$

$$U=\int\int d\mathbf{r}_1d\mathbf{r}_2\frac{e^2|\phi(\mathbf{r}_1)|^2|\phi(\mathbf{r}_2)|^2}{4\pi\varepsilon|\mathbf{r}_1-\mathbf{r}_2|}=\frac{\sqrt{2\pi}e^2}{4\pi\varepsilon d}, \tag{9}$$

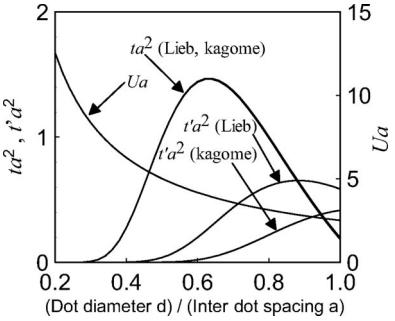

FIG. 5. The nearest- and the next-nearest-neighbor transfer energies t, t' and on-site Coulomb energy U in the dot model as a function of d/a. Energy and length are scaled in units of the effective rydberg constant Ry* and the effective Bohr radius a_B^* (see text).

where ε is the dielectric constant.[32] Note that the minus sign of the integral in Eq. (8) comes from the definition of the transfer energy in Eq. (1). Here, the nearest-neighbor transfer t is calculated for $\mathbf{R}_i=(0,0)$ and $\mathbf{R}_j=(a,0)$, and the next-nearest-neighbor transfer t' is for $\mathbf{R}_i=(a,0)$ and $\mathbf{R}_j=(0,a)$ in the Lieb lattice and $\mathbf{R}_i=(a,0)$ and $\mathbf{R}_j=(a/2,\sqrt{3}a/2)$ in the *kagomé* lattice. The Coulomb energy can be analytically integrated, but the transfer integral is evaluated numerically from Eqs. (6) and (7). Figure 5 shows the calculated transfer and the on-site Coulomb energy as a function of the dot diameter. Here, we adapt the effective atomic units $\hbar^2/2m^*=e^2/4\pi\varepsilon=1$. In these units, energy and length are scaled in units of the effective rydberg constant $\mathrm{Ry}^*=13.6$ eV $\times(m^*/m_0)/(\varepsilon/\varepsilon_0)^2$ and the effective Bohr radius $a_B^*=0.53$ Å $\times(\varepsilon/\varepsilon_0)/(m^*/m_0)$, where m_0 and ε_0 are the mass of a bare electron and the dielectric constant in vacuum. In our dot model, the contribution from terms such as $\langle\phi(\mathbf{0})|v(\mathbf{R}_i)|\phi(\mathbf{R}_j)\rangle$ $(\mathbf{R}_i\neq\mathbf{0},\ \mathbf{R}_j)$ is negligible in Eq. (8), and the transfer energy is determined by the distance between the nearest-neighboring dots, i.e., $t\simeq\langle\phi(\mathbf{0})|\{\mathbf{p}^2/2m^*+v(\mathbf{0})+v(\mathbf{R}_i)\}|\phi(\mathbf{R}_i)\rangle$. Therefore, the transfer energies for the Lieb and *kagomé* lattices are almost identical within the width of drawn lines in Fig. 5. On the other hand, t' for the Lieb lattice is larger than that for the *kagomé* lattice, because of the difference in the distance of the next-nearest-neighbor dots, i.e., $|\mathbf{R}_i-\mathbf{R}_j|=\sqrt{2}a$ for the Lieb lattice and $|\mathbf{R}_i-\mathbf{R}_j|=\sqrt{3}a$ for the *kagomé* lattice. For $d/a\lesssim0.5$, t' is much smaller than t and is negligible. It is noted that t is always smaller than U when the interdot spacing $a\gtrsim0.1$, which is usually realized in the present fabrication technology.

In realistic dot arrays formed by a negatively biased gate electrode depleting the underneath two-dimensional electron gas, the interdot spacing is usually fixed and cannot be changed. By modifying the gate voltage, the dot diameter can be changed. To simulate this, we evaluate t, t', and U from Eqs. (8) and (9) for a fixed interdot spacing ($a=0.5$, 1, 5, 10) and calculate the energy difference as a function of dot diameter as shown by the closed symbols in Fig. 6. The energy difference is appreciable for $0.3\lesssim d/a\lesssim0.7$. For $a>0.5$, t is always smaller than U. In this strongly correlated region, the energy difference ΔE has the dependence of $\Delta E\sim t^2/U\sim1/a^3$ for the Lieb lattice, and $\Delta E\sim t\sim1/a^2$ for the *kagomé* lattice. For $d/a\gtrsim0.6$, ΔE rapidly decreases, since t' becomes significantly large and the ground state becomes paramagnetic. In Fig. 6, ΔE for $t'=0$ is also plotted. When $d/a\gtrsim0.6$, ΔE for $t'=0$ monotonically decreases but does not become negative, since the ground state is always ferromagnetic for $t'=0$. It is noted that, when ΔE takes a peak around $d/a=0.5-0.6$, the effect of t' is negligible and ΔE is not affected by t'.

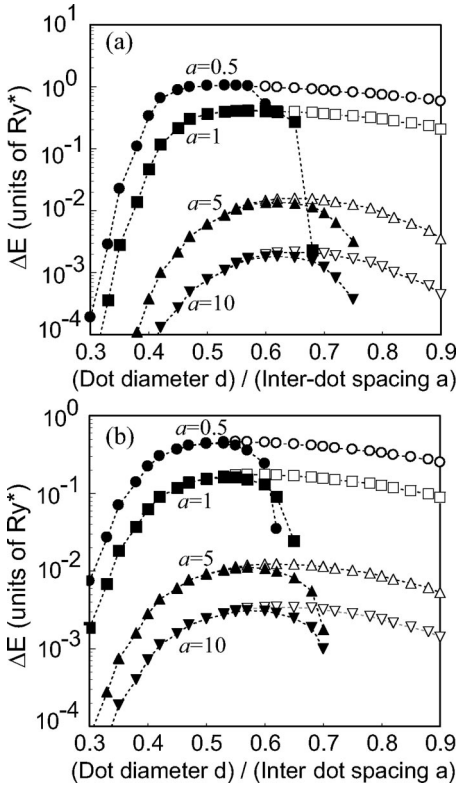

FIG. 6. Energy difference $\Delta E=E(S=0)-E(S=2)$ as a function of dot diameter d for (a) the Lieb and (b) the *kagomé* lattices for various interdot spacing a in the dot model represented by solid symbols. Open symbols represent the energy difference when we neglect the next-nearest-neighbor transfer t'.

In Table I, we estimate ΔE for dot arrays of various sizes. We consider GaAs, InAs, and Si dots and assume $a=2d$. For dots with a spacing of 100 nm which is available within the present fabrication technology, ΔE is of the order of several hundreds millidegrees Kelvin and we can expect that ferromagnetism can be observable in the dilution temperature region. For dots of spacing of 5 nm, ΔE is as high as a few tens of Kelvin.

V. DISCUSSION

There are several advantages of using semiconductors in making artificial crystals. First, the lattice structure can be widely chosen. One can fabricate a lattice structure that does not exist in nature. Second, interdot coupling and the electron filling can be separately modified. This is possible if the interdot coupling is modified mainly by the front-gate electrode on top of the two-dimensional electron gas and the electron filling is modified mainly by the back-gate elec-

TABLE I. Estimated energy difference $\Delta E = E(S=0) - E(S=2)$ (K) between the ground state with spin 2 and the lowest excited state with spin 0 for dot arrays of the Lieb and *kagomé* lattices of typical interdot spacing $a=5$, 10, 50, and 100 nm and dot diameter $a/2$. We consider GaAs dots ($m^*/m_0=0.067$, $\varepsilon/\varepsilon_0=12.4$, Ry$^*=6$ meV, $a_B^*=10$ nm), InAs dots ($m^*/m_0=0.02$, $\varepsilon/\varepsilon_0=12.4$, Ry$^*=1.8$ meV, $a_B^*=34$ nm), and Si dots ($m^*/m_0=0.2$, $\varepsilon/\varepsilon_0=12$, Ry$^*=19$ meV, $a_B^*=3$ nm).

	ΔE (K) for Lieb lattice				ΔE (K) for *kagomé* lattice			
Spacing a	5 nm	10 nm	50 nm	100 nm	5 nm	10 nm	50 nm	100 nm
GaAs	76	26	0.5	0.06	31	11	0.6	0.2
InAs	90	43	3.5	0.6	45	19	1.7	0.5
Si	27	4.5	0.04	0.005	15	4.3	0.2	0.05

trode. The controllability of electron filling enables us to switch ferromagnetism on and off. It would be better to use the *kagomé* lattice in order to switch the ferromagnetism because the ferromagnetic ground state appears in a wide range of electron filling as shown in Fig. 3(b). The effect of a magnetic field in the *kagomé* lattice is also very interesting because the flat band is destroyed by the threaded magnetic flux. It has been found that a giant negative magnetoresistance and ferromagnetic–paramagnetic transition induced by a magnetic field occur in the *kagomé* dot lattice.[33] Recently, the present authors have proposed a simple way to realize the *kagomé* dot lattice within the present fabrication technology.[34] It has been shown that a network of quantum wires effectively acts as a *kagomé* lattice where electrons are well localized at the cross points of two wires. This kind of *kagomé* network has been already available in quantum wires formed by a selective area growth technique.[35] This method of making a *kagomé* dot lattice provides us with a chance to observe the flat-band ferromagnetism in experiment.

One may think that a finite magnetization does not appear at finite temperatures in two dimensions because of the absence of long-range order according to the Mermin-Wagner theorem.[36] However, it has been shown that the spin-spin correlation length ξ in the spin-1/2 Heisenberg model on a 2D square lattice exponentially grows as $\xi \sim \exp(J/T)$ as temperature decreases although the (antiferromagnetic) spin-spin correlation decays as $\langle \mathbf{S}_0 \cdot \mathbf{S}_r \rangle \propto \exp(-r/\xi)$.[37] Then, the spin-spin correlation length ξ can be macroscopically large at low temperatures. For example, at $T=0.1J$, ξ is 10^4 times larger than the lattice spacing. Noticing that the Hubbard model in the Lieb lattice for $U/t \gg 1$ at the half-filling is reduced to the Heisenberg model with the same antiferromagnetic coupling ($J=4t^2/U$) as in the square lattice, the temperature dependence of ξ also holds for the Lieb lattice. In contrast to the square lattice, a finite magnetization can appear in the Lieb lattice because the numbers of sites in two sublattices are different. As for the *kagomé* lattice, there has been no theory, to our best knowledge, on spin waves to date and the effect of thermal fluctuation on the spin-spin correlation is still unknown. At least, a finite magnetization can be expected in the Lieb lattice even in two dimensions as long as the sample size is smaller than the spin-spin correlation length. Moreover, considering $J \sim \Delta E$, our estimation of the transition temperature in Fig. 6 is qualitatively justified.

Although a finite magnetization is expected in two dimensions, its value will be quite small in 2D dot arrays, since the lattice constant ($\gtrsim 10$ nm) of dot arrays is about more than a hundred times larger than that of the conventional ferromagnetic materials and the expected magnetization per area will be significantly reduced. For example, the expected magnetization of dot arrays of the interdot spacing a with spin $S=1/2$ per unit cell is $g\mu_B S/a^3 \sim 0.1$ G for $a=10$ nm and $\sim 10^{-4}$ G for $a=100$ nm, where $\mu_B = e\hbar/2m$ is the Bohr magneton and $g \simeq 2$ is a gyromagnetic ratio. To measure the magnetic moment directly, a very sensitive detector such as a superconducting quantum interference device magnetometer would be required. A more convenient way to detect the magnetization directly will be to measure the anomalous Hall resistivity which is proportional to the magnetization of the sample and is added to the normal Hall resistivity proportional to the external magnetic field. This method will only be applicable when the magnetization is larger than 0.01 G ($a \lesssim 10$ nm). On the other hand, magnetoresistance measurement is rather an indirect way to detect the magnetization. When the magnetic field is increased, the insulating ferromagnetic state turns into the metallic paramagnetic one in the *kagomé* lattice at the half-filled flat-band.[33] The magnitude of the magnetization could not be estimated only from the magnetoresistance measurement, although the ferromagnetic–paramagnetic phase transition could be detected.

The advantage of using semiconductors in realizing ferromagnetism exists not only in making semiconducting ''permanent magnets.'' As we mentioned, the controllability of the magnetic property by changing the electron filling and the magnetic field will make dot lattices useful in electronic devices such as memories, sensors, and magnetic heads since only semiconductor materials such as Si and GaAs are contained. Magnetic devices can be fabricated without using any magnetic elements such as iron and manganese which are incompatible with the conventional large-scale-integrated circuit (LSI) fabrication process.

By extending the idea of dot superlattices, one can think of other interesting possibilities for artificial materials. Thanks to the rapid progress in semiconductor nanotechnology, we can expect that various interesting electric properties which have been observed in conventional materials may be realized also in dot superlattices. One of the most fascinating examples is high-temperature (high-T_c) superconductivity.

High-temperature *d*-wave superconductivity in a repulsive Hubbard model has been predicted.[38] Although the energy scales or the transition temperature is a hundred times smaller than the conventional CuO_2 high-T_c superconductors ($T_c \sim 100$ K), superconductivity in semiconductor dot arrays might be possible, because the estimated transition temperature using the predicted expression is $T_c \simeq 0.01t \sim 1$ K for $a = 2d = 10$ nm GaAs dots. It has been shown that, in other types of lattices, the transition temperature becomes much higher.[39,40] It would be very interesting if superconductivity (or at least the Kosterlitz-Thouless-Berezinskii transition) could be realized in semiconductors. Other types of lattice structures would also be fascinating, such as a ladder structure realized in copper oxide materials, where various interesting properties have been observed such as the spin gap and superconductivity.[41–43] Optical properties of the dot arrays would also be interesting, since the large density of states in the flat band will significantly affect photoluminescence or laser characteristics.

VI. CONCLUSIONS

Flat-band ferromagnetism in quantum dot arrays has been theoretically discussed. We considered dot arrays on the Lieb and *kagomé* lattices which are known to exhibit flat-band ferromagnetism. The tight-binding calculation showed that the next-nearest-neighbor transfer t' destroys the flat subband. We performed the exact diagonalization of the Hubbard Hamiltonian and calculated the energy difference between high-spin and low-spin states. This energy difference represents a qualitative estimate of the transition temperature of ferromagnetic and paramagnetic states in a macroscopic sample. The energy difference becomes smaller as the next-nearest-neighbor transfer t' increases. It was shown that, although the ferromagnetic ground state is easily broken down by t' in the weak correlation region ($t \gg U$), it is robust against t' in the strong correlation region ($U \gg t$).

We calculated the size dependence of the energy difference in a realistic dot model. We found that, although the next-nearest-neighbor transfer destroys the ferromagnetism when the dot diameter approaches the interdot spacing, it does not affect the peak value of the energy difference or the transition temperature when the dot diameter decreases. We argued that the flat-band ferromagnetism can be observable in dot arrays fabricated using the present technology. We suggested other interesting possibilities for artificial material design using quantum dot superlattices.

ACKNOWLEDGMENTS

We would like to thank K. Kuroki and K. Kusakabe for valuable discussions. We also thank S. Ishihara for his encouragement and support of the present work. This work was partly supported by the NEDO International Joint Research Grant, the JSPS Research for the Future Programs in the Area of Atomic Scale Surface and Interface Dynamics, and the Telecommunication Advancement Organization.

[1] U. Meirav and E. B. Foxman, Semicond. Sci. Technol. **10**, 255 (1995), and references therein.
[2] D. V. Averin and K. K. Likharev, *Single Charge Tunnelling* (Plenum Press, New York, 1992), Vol. 294, p. 311, and references therein.
[3] D. Loss and D. P. DiVincenzo, Phys. Rev. A **57**, 120 (1998).
[4] C. Livermore, C. H. Crouch, R. M. Westervelt, K. L. Campman, and A. C. Gossard, Science **274**, 1332 (1996).
[5] R. H. Blick, R. J. Haug, J. Weis, D. Pfannkuche, K. v. Klitzing, and K. Eberl, Phys. Rev. B **53**, 7899 (1996).
[6] Y. Arakawa and H. Sakaki, Appl. Phys. Lett. **40**, 939 (1992).
[7] L. Goldstein, F. Glas, J. Y. Marzin, M. N. Charasse, and G. Le Roux, Appl. Phys. Lett. **47**, 1099 (1985).
[8] J. Temmyo, E. Kuramochi, T. Tamamura, and H. Kamada, J. Cryst. Growth **195**, 516 (1998).
[9] C. S. Lent, P. D. Tougaw, and W. Porod, Appl. Phys. Lett. **62**, 714 (1993); C. S. Lent and P. D. Tougaw, J. Appl. Phys. **74**, 6227 (1993).
[10] P. D. Tougaw and C. S. Lent, J. Appl. Phys. **80**, 4722 (1996).
[11] J. B. Khurgin, F. Jin, and A. Obeidat, Appl. Phys. Lett. **73**, 3944 (1998); Superlattices Microstruct. **24**, 133 (1998).
[12] J. Kolehmainen, S. M. Reimann, M. Koskinen, and M. Manninen, Eur. Phys. J. B **13**, 731 (2000).
[13] H. Tamura, K. Shiraishi, and H. Takayanagi, Jpn. J. Appl. Phys., Part 2 **39**, L241 (2000).
[14] A. Sugimura, Jpn. J. Appl. Phys., Part 2 **29**, L2463 (1990).
[15] E. H. Lieb, Phys. Rev. Lett. **62**, 1201 (1989).
[16] A. Mielke, J. Phys. A **24**, L73 (1991).
[17] Another important type of lattice showing flat-band ferromagnetism has been given by H. Tasaki, Phys. Rev. Lett. **69**, 1608 (1992).
[18] K. Kusakabe and H. Aoki, Phys. Rev. Lett. **72**, 144 (1994).
[19] K. Kusakabe and H. Aoki, Physica B **194-196**, 215 (1994).
[20] K. Penc, H. Shiba, F. Mila, and T. Tsukagoshi, Phys. Rev. B **54**, 4056 (1996).
[21] H. Sakamoto and K. Kubo, J. Phys. Soc. Jpn. **65**, 3732 (1996).
[22] Y. Wanatabe and S. Miyashita, J. Phys. Soc. Jpn. **66**, 2123 (1997); **66**, 3981 (1997).
[23] N. Shima and H. Aoki, Phys. Rev. Lett. **71**, 4389 (1993).
[24] M. Fujita, T. Umeda, and M. Yoshida, Phys. Rev. B **51**, 13 778 (1995).
[25] M. Fujita, K. Wakabayashi, K. Nakada, and K. Kusakabe, J. Phys. Soc. Jpn. **65**, 1920 (1996).
[26] K. Kusakabe, K. Wakabayashi, M. Igami, K. Nakada, and M. Fujita, Mol. Cryst. Liq. Cryst. **305**, 445 (1997).
[27] A. Yajima, M. Tsukada, S. Watanabe, M. Ichimura, Y. Sawa, T. Onogi, and T. Hashizume, Phys. Rev. B **60**, 1456 (1999).
[28] R. Arita, K. Kuroki, H. Aoki, A. Yajima, M. Tsukada, S. Watanabe, M. Ichimaru, T. Onogi, and T. Hashizume, Phys. Rev. B **57**, R6854 (1998).
[29] S. Okada and A. Oshiyama, Phys. Rev. B **62**, R13 286 (2000).
[30] A. Kawaharazuka, T. Saku, Y. Hirayama, and Y. Horikoshi, J. Appl. Phys. **87**, 952 (2000).

[31] R. Fleischmann, T. Geisel, and R. Ketzmerick, Phys. Rev. Lett. **68**, 1367 (1992).
[32] A simple one-dimensional microscopic confinement model has been discussed by R. Kotlyar and S. Das Sarma, Phys. Rev. B **56**, 13 235 (1997); C. A. Stafford, R. Kotlyar, and S. Das Sarma, *ibid.* **58**, 7091 (1998).
[33] T. Kimura, H. Tamura, K. Shiraishi, and H. Takayanagi, Phys. Rev. B (to be published).
[34] K. Shiraishi, H. Tamura, and H. Takayanagi, Appl. Phys. Lett. **78**, 3702 (2001).
[35] K. Kumakura, J. Motohisa, and T. Fukui, J. Cryst. Growth **170**, 700 (1997).
[36] N. D. Mermin and H. Wagner, Phys. Rev. Lett. **17**, 1133 (1966).
[37] E. Manousakis, Rev. Mod. Phys. **63**, 1 (1991).
[38] See e.g., T. Dahm and L. Tewordt, Phys. Rev. B **52**, 1297 (1995); J. J. Deisz, D. W. Hess, and J. W. Serene, Phys. Rev. Lett. **76**, 1312 (1996).
[39] K. Kuroki and R. Arita, Phys. Rev. B **64**, 024501 (2001).
[40] T. Kimura, H. Tamura, K. Kuroki, K. Shiraishi, H. Takayanagi, and R. Arita (unpublished).
[41] E. Dagotto, J. Riera, and D. Scalapino, Phys. Rev. B **45**, 5744 (1992).
[42] E. Dagotto and T. M. Rice, Science **271**, 618 (1996).
[43] M. Uehara, T. Nagata, J. Akimitsu, H. Takahashi, T. Mori, and K. Kinoshita, J. Phys. Soc. Jpn. **65**, 2764 (1996).